Mechanisms for millennial-scale global synchronization during the last glacial period

A. Timmermann,[1] U. Krebs,[2] F. Justino,[3] H. Goosse,[4] and T. Ivanochko[5]

Received 8 September 2004; revised 5 May 2005; accepted 10 June 2005; published 27 October 2005.

[1] Global climate during the last glacial period was punctuated by abrupt warmings and occasional pulses of freshwater into the North Atlantic that disrupted deepwater production. These massive freshwater pulses known as Heinrich events arose, in part, from instabilities within the Laurentide ice sheet. Paleoevidence from the North Atlantic suggests that these events altered the production of deep water and changed downstream climate throughout the Northern Hemisphere. In the tropical western Pacific sea, surface temperatures and salinity varied together with ocean and climate changes at high latitudes. Here we present results from coupled modeling experiments that shed light on a possible dynamical link between the North Atlantic Ocean and the western tropical Pacific. This link involves a global oceanic standing wave pattern brought about by millennial-scale glacial density variations in the North Atlantic, atmospheric teleconnections triggered by meridional sea surface temperature gradients, and local air-sea interactions. Furthermore, our modeling results are compared with hydrological records from the Cariaco basin, the Indian Ocean, the Sulu Sea, and northern Australia.

Citation: Timmermann, A., U. Krebs, F. Justino, H. Goosse, and T. Ivanochko (2005), Mechanisms for millennial-scale global synchronization during the last glacial period, *Paleoceanography*, *20*, PA4008, doi:10.1029/2004PA001090.

1. Introduction

[2] Proxy records covering marine isotope stage 3 (MIS3) (60,000–25,000 years B.P.) reveal that the amplitude of climatic changes in the Northern Hemisphere during the last glacial period was greater than it has been during the Holocene. The last glacial period was characterized by [*Dansgaard et al.*, 1993] Dansgaard-Oeschger (DO) stadial-interstadial (cold-warm) transitions that involved abrupt temperature variations over Greenland of up to 16K [*Lang et al.*, 1999; *Severinghaus and Brook*, 1999]. In addition, this period was punctuated by Heinrich events that produced thick layers of ice rafted debris (IRD) in marine sediments throughout the North Atlantic [*Heinrich*, 1988]. Heinrich events, massive surges of icebergs originating from the glacial ice sheets and shelves, were accompanied by cold conditions in the North Atlantic region, warm episodes in Antarctica [*Blunier and Brook*, 2001] and by increases of global sea level of up to 30 m [*Yokoyama et al.*, 2001; *Sidall et al.*, 2003]. Furthermore, the associated millennial-scale North Atlantic density changes appear to have slowed or even terminated the meridional overturning circulation in the North Atlantic [*Keigwin and Lehman*, 1994; *Knutti et al.*, 2004]. While the amount of proxy data documenting these transitions in the tropics is growing [e.g., *Schultz et al.*, 1998; *Peterson et al.*, 2000; *Turney et al.*, 2004; *Ivanochko et al.*, 2005], the physical mechanisms responsible for these characteristic millennial-scale variations and their global teleconnections have not been fully disentangled.

[3] On the basis of a tropical model of intermediate complexity, *Cane and Clement* [1999] argued that "abrupt" Northern Hemispheric transitions can be triggered remotely from abrupt orbitally driven regime transitions of the El Niño–Southern Oscillation (ENSO). Evidence for tropical changes on millennial rather than precessional timescales was recently provided by salinity reconstructions from the Pacific warm pool area [*Stott et al.*, 2002]. It was shown [*Stott et al.*, 2002] that millennial-scale variations of the warm pool salinity varied with DO events in the North Atlantic (see Figure 1). Salinities decreased during interstadials and reversed during stadials [*Stott et al.*, 2002]. (Note, however, that the exact phase difference between these curves is uncertain and the apparent correlation between stadials and saline conditions in the warm pool may be an artefact of using the joint GISP2 timescale, assuming already a certain type of wiggle matching and correlation.) Because atmospheric teleconnections from the North Atlantic to the warm pool area were considered to be unlikely candidates to explain the observed correlation between the tropics and the northern extratropics, *Stott et al.* [2002] suggested the millennial-scale variations in the North Atlantic were forced by ocean/atmospheric teleconnections analogous to the modern interannual variability associated with ENSO [*Livezey et al.*, 1997]. As the changes in the North Atlantic and tropical Pacific occurred over millennia the term super-ENSO was used to distinguish these changes from those associated with the modern

[1] International Pacific Research Center, University of Hawai'i, Honolulu, Hawaii, USA.
[2] Leibniz Institut für Meereswissenschaften, IfM-GEOMAR, Kiel, Germany.
[3] Department of Physics, University of Toronto, Toronto, Ontario, Canada.
[4] Institut d'Astronomie et de Géophysique, Université Catholique de Louvain, Louvain-la-Neuve, Belgium.
[5] Department of Earth and Ocean Sciences, University of British Columbia, Vancouver, British Columbia, Canada.

0883-8305/05/2004PA001090

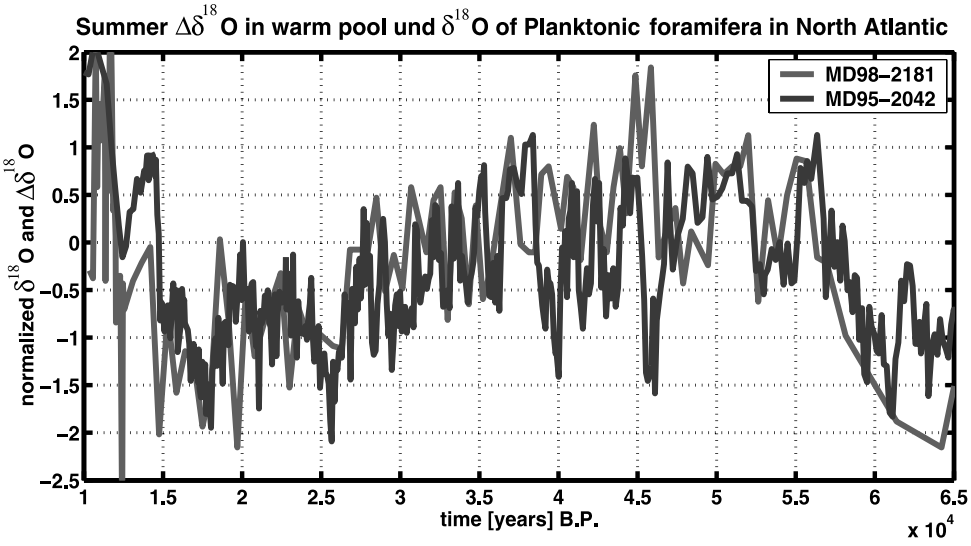

Figure 1. Extratropical-tropical connections: normalized and inverted time series of $\Delta\delta^{18}O$ of planktonic foramanifera (red) in the Pacific warm pool core MD98-2181 [*Stott et al.*, 2002]. The largest $\Delta\delta^{18}O$ variations for Globigerinoides ruber represent local salinity variations and are coherent with the Dansgaard-Oeschger (DO) cycles, as recorded in the normalized $\delta^{18}O$ of planktonic foraminifera (blue) sampled off the Iberian margin [*Shackleton et al.*, 2000]. Both records are shown on the Greenland Ice Sheet Project 2 (GISP2) timescale [*Blunier and Brook*, 2001]. See color version of this figure at back of this issue.

interannual variability. In contrast to *Stott et al.* [2002] a recent analysis of a high-resolution record of surface moisture [*Turney et al.*, 2004] in Northern Australia suggests a link between an El Niño–like climate change pattern and interstadials in the North Atlantic, rather than a link between warm eastern equatorial Pacific SST and stadial conditions in the North Atlantic. In both cases variations of salinity or precipitation have been connected to eastern equatorial temperature anomalies, rather than with oceanic changes and/or changes of the meridional position of the Intertropical Convergence Zone (ITCZ). Our study presents evidence for a mechanism that can explain the link between tropical Pacific salinity and temperature and North Atlantic density anomalies triggered by either Heinrich or Dansgaard-Oeschger events. This mechanism involves panoceanic meridional changes in the position and strength of the ITCZ and baroclinic adjustments in the global ocean.

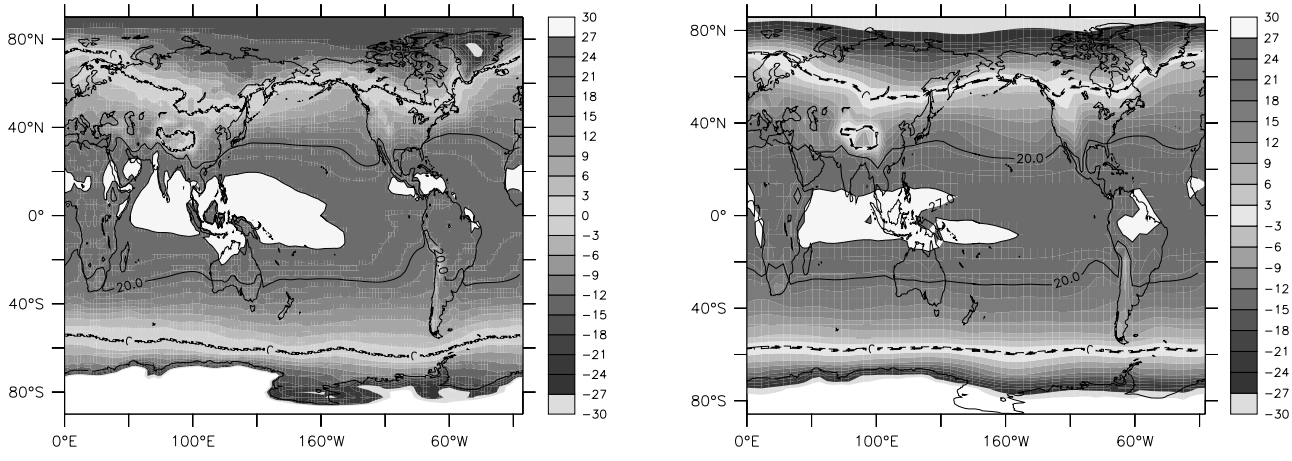

Figure 2. (left) Averaged ECMWF Reanalysis Data-Assimilation 40 (ERA40) 2-m temperature, representing an estimate of the observed temperatures. (right) Simulated averaged 2-m temperature for a 280 ppm 2000-year-long control (CTR) simulation using ECBilt-Clio. See color version of this figure at back of this issue.

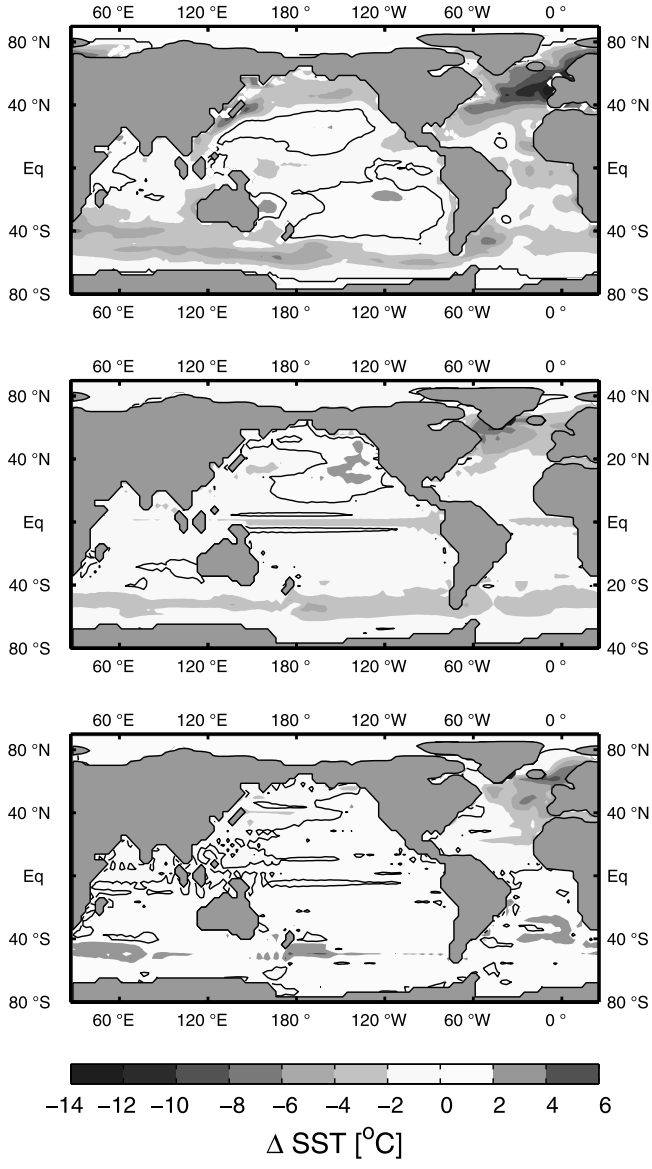

Figure 3. Reconstructed and simulated glacial sea surface temperature (SST) anomalies. (top) Difference between reconstructed North Atlantic GLAMAP [*Sarnthein et al.*, 2003] and Pacific and Indian oceans [*CLIMAP*, 1981] sea surface temperature (time average of February and August) for the Last Glacial Maximum (LGM) and the present-day SST [*CLIMAP*, 1981]. (middle) Sensitivity of the simulated annual mean SST to glacial boundary conditions as quantified by the difference of the equilibrated time-mean SST of the LGM experiment and the preindustrial CTR experiment. (bottom) Simulated SST difference between a collapsed thermohaline circulation (THC) state during the LGM (time average of years 200–300 in experiment meltwater (MW)) and normal LGM conditions. See color version of this figure at back of this issue.

[4] In section 2 we briefly describe the five modeling experiments conducted and analyzed here. Section 3 studies the atmospheric teleconnections of a shutdown of the meridional overturning circulation. Section 4 focuses on the oceanic component of the global teleconnection. The study concludes with a summary of our main results and a discussion thereof (section 5).

2. Model Experiments

[5] The analysis is based on a series of global atmosphere-ocean-sea ice model simulations performed with the coupled model ECBilt-Clio. The atmospheric component ECBILT [*Opsteegh et al.*, 1998] of our coupled model is a three-layer model with a quasi-geostrophic adiabatic core [*Marshall and Molteni*, 1993] and a set of physical parameterizations for the hydrological cycle [*Held and Suarez*, 1978] and a partly linearized radiation code. It runs in T21 triangular truncation, which corresponds to an approximate resolution of 5.6° in both latitude and longitude. The coupled ocean–sea ice model CLIO [*Goosse and Fichefet*, 1999] is based on the primitive equations using a free surface and thermodynamic/dynamic assumptions, respectively. A parameterization of vertical mixing [*Goosse et al.*, 1999] is used that represents a simplification of the [*Mellor and Yamada*, 1982] 2.5-level turbulence closure scheme. The ocean model CLIO also includes mixing along isopycnals and it captures the effect of mesoscale eddies on transport [*Gent and McWilliams*, 1990]. Furthermore, a parameterization for the dense water flow down topographic features [*Campin and Goosse*, 1999] is employed. The horizontal resolution of CLIO is 3°, and there are 20 unevenly spaced vertical levels in the ocean. The individual models are coupled by exchanging fluxes of momentum, freshwater, and heat. The simulations are performed with weak freshwater-flux corrections, which mostly affect the North Atlantic region. The model is freely available from http://www.knmi.nl/onderzk/CKO/ecbilt.html. In the standard model setup an imbalance in the global, interannual freshwater budget is compensated globally for numerical reasons. However, in our experiment the imbalance associated with surging icebergs is intended and thus not compensated.

[6] A 2000-year-long control simulation (CTR) represents preindustrial climate with an atmospheric CO_2 concentration of 0.28% [*Timmermann et al.*, 2004]. Figure 2 (right) shows the simulated 2-m air temperature for preindustrial conditions. It compares quite well with the ECMWF Reanalysis Data-Assimilation 40 (ERA40) simulated 2-m temperatures (Figure 2, left), although small differences in the CO_2 base state have to be considered.

[7] The Last Glacial Maximum (LGM) simulation [*Timmermann et al.*, 2004] performed here utilizes the [*Peltier*, 1994] ice sheet topography of about 21,000 years ago, an ice sheet–albedo mask, reduced CO_2 concentrations (200 ppm), modified orbital forcing, and a LGM vegetation index [*Crowley and Baum*, 1997] for which the deforested soils and plant cover are replaced by their respective glacial albedo. The inclusion of the ice sheet increases the albedo by more than 60% in North America and Europe. The associated changes in the river runoff and sea level drop have not been included here. The surface climate of the 2000-year-long LGM simulation equilibrates after about 500 years. The simulated North Atlantic sea surface temperature (SST) differences between LGM and CTR

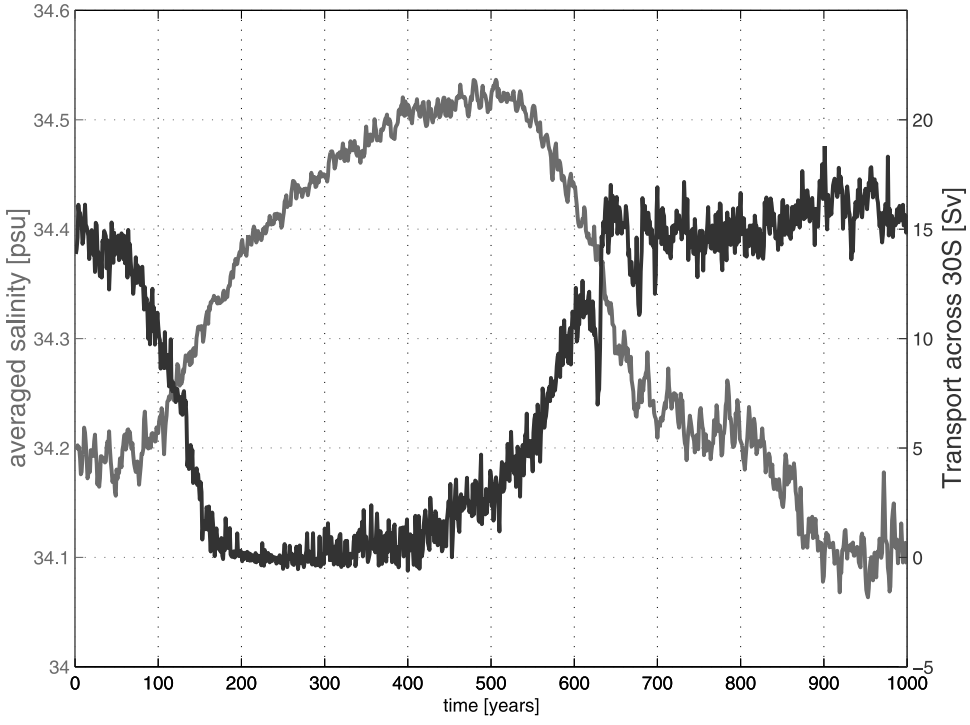

Figure 4. North Atlantic–tropical Pacific teleconnections. Simulated time series of the meridional ocean transport across 30°S in the North Atlantic (Sv = $10^6 \times m^3/s$) (blue) and area-averaged salinity (psu) in the Pacific warm pool (15°S–15°N, 120°E–160°E) area are shown. See color version of this figure at back of this issue.

(Figure 3) are smaller than in recent SST reconstructions [*Sarnthein et al.*, 2003]. Simulated LGM tropical sea surface temperature anomalies attain minimal values of −2 K to −3 K, consistent with alkenone reconstructions of *Lyle et al.* [1992] and *Bard* [2001] and the cold tongue record of *Lea et al.* [2000]. However, our modeling results exhibit a cold bias in the tropical Pacific compared to the *Climate: Long-Range Investigation, Mapping, and Prediction* (*CLIMAP*) [1981] reconstruction and the Galapagos record [*Koutavas et al.*, 2002] and a warm bias with respect to *Hostetler and Mix* [1999]. The simulated positive SST anomaly in the northern Pacific (Figure 3) can be attributed to an overall weakening of the atmospheric westerlies in the North Pacific [*Timmermann et al.*, 2004]. It bears some similarities with the CLIMAP reconstruction and a recent LGM modeling result [*Kitoh et al.*, 2001].

[8] At the core of our analysis is a transient meltwater (MW) experiment, which mimics the response of the glacial climate to a North Atlantic density perturbation, such as the one caused for instance by the Heinrich event 2. A Gaussian-shaped (half width 100 years) freshwater flux anomaly of 1.2 m/year (maximum value) is injected homogenously into the North Atlantic between 40°–60°N. This length is consistent with the most recent model-based estimates of *Roche et al.* [2004]. The equivalent global sea level rise of this hydrological forcing amounts to about 8 m.

[9] In order to study the atmospheric teleconnections more in detail two other meltwater experiments have been conducted. In MW1 the atmosphere does not respond to SST anomalies triggered by the THC shutdown anywhere. In this sense the atmosphere is generating variability and air-sea fluxes based on global LGM SST climatology obtained from the LGM experiment. The atmosphere is decoupled from the actual ocean anomaly state globally, and the ocean is driven by simulated atmospheric heat, freshwater, and momentum fluxes. The experiment MW2 is very similar to MW1, with the main difference that the atmosphere in MW2 is insensitive to North Atlantic SST anomalies induced by the shutdown of the meridional overturning circulation, whereas it responds to SST anomalies elsewhere.

[10] The physical mechanisms that generate DO events have not been disentangled yet. Some recent modeling evidence [*Knutti et al.*, 2004] suggests that DO events are associated with millennial-scale density-driven switches of the meridional overturning circulation in the North Atlantic. However, the origin of the initial density changes has not been identified unambiguously. They may be generated by internal oceanic processes [*Timmermann et al.*, 2003] or may be due to external forcing [*Rahmstorf*, 2003]. Further changes of the sea ice extent may help to amplify oceanic changes into relevant atmospheric changes. Hence we assume that the diagnosed link between North Atlantic density anomalies and climate conditions in the Indian and Pacific oceans holds for stadial-interstadial transitions both with and without the involvement of Heinrich events.

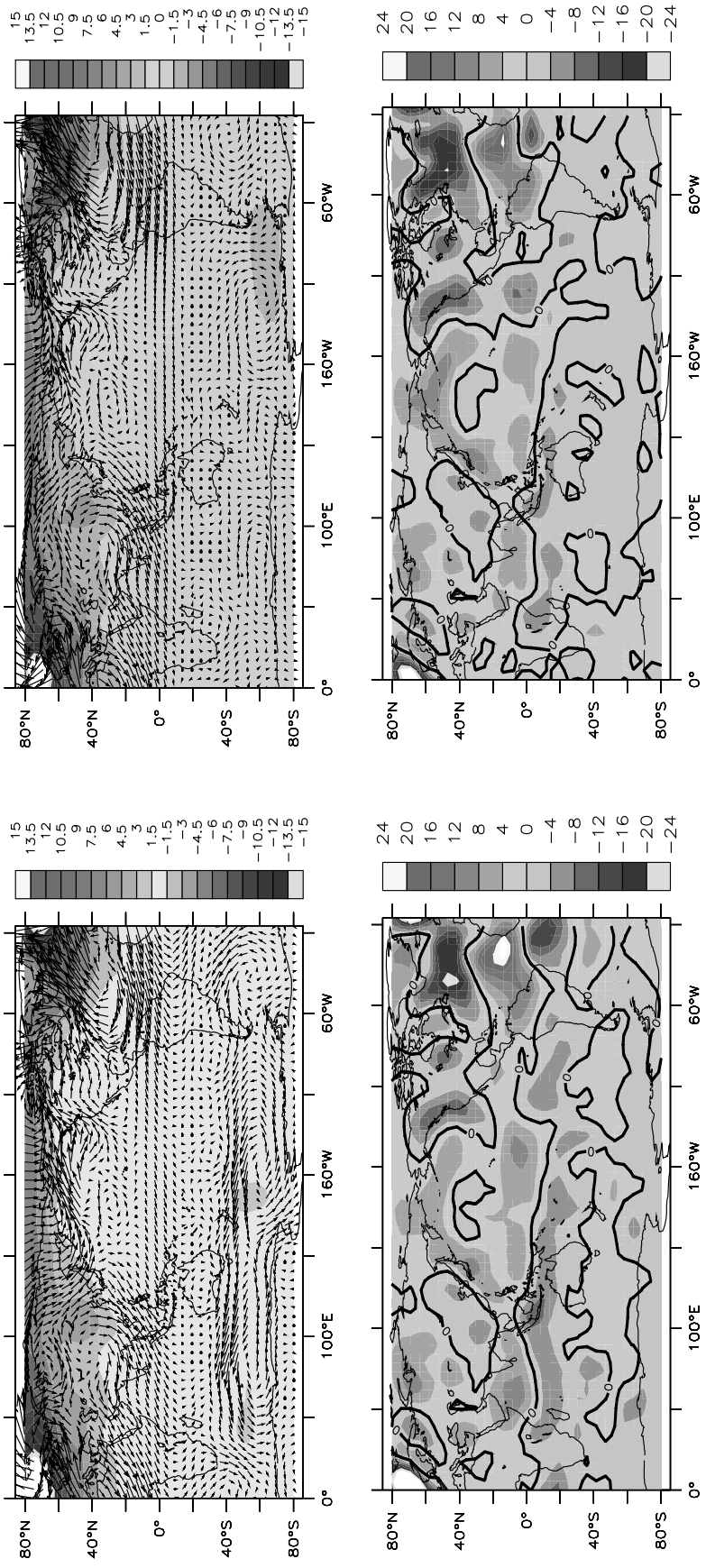

Figure 5. Atmospheric response to Heinrich event. (top) Difference of time-averaged wind stress (vectors) and temperature (K) (shading) fields of (left) MW and LGM and (right) MW and MW2. The time average represents the THC shutdown state and is computed from the simulation years 250–300. (bottom) Same as top plots but for evaporation minus precipitation (cm/yr). See color version of this figure at back of this issue.

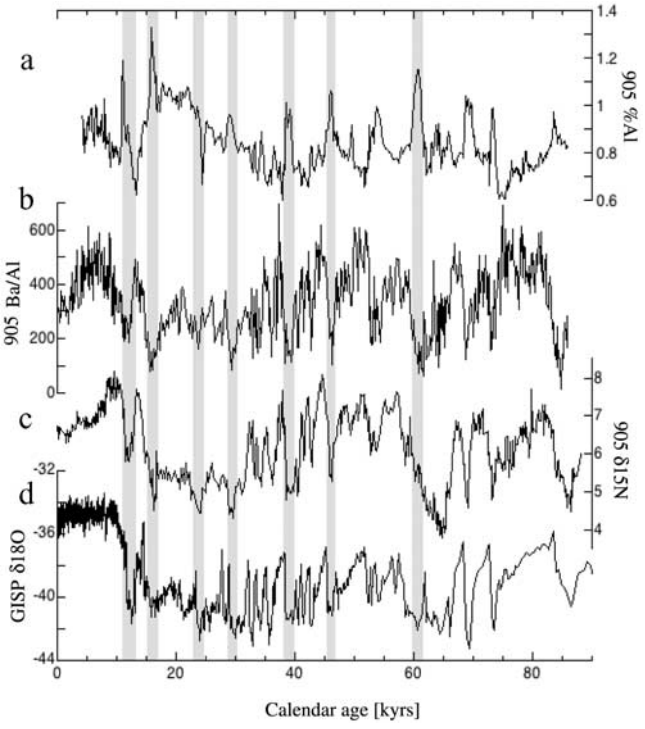

Figure 6. Variations in the strength of the Arabian monsoon compared to changes in Greenland paleotemperature. The Younger Dryas (YD) and Heinrich events (H1–H6) are represented by shaded bands. Site 905 (10°46′N, 51°57′E) [*Ivanochko et al.*, 2005] is located in the western Arabian Sea. (a) Increased percent of Al in Site 905 indicating increased dustiness and a more arid continent during periods of diminished monsoon rainfall. (b) Ba (ppm) normalized to percent of Al (Ba/Al) reflecting the biogenic Ba that is delivered to the sediments in association with the flux of organic matter. At site 905, increased productivity occurs when the strength of monsoon-induced coastal upwelling increases [*Honjo et al.*, 1999]. (c) Core 905 nitrogen isotopic record. Monsoon-induced productivity mediates denitrification in the intermediate waters of the Arabian Sea. Larger $\delta^{15}N$ values suggest increased monsoon strength [*Ivanochko et al.*, 2005]. (d) Past changes in Greenland temperature inferred from the oxygen isotope record from GISP2 [*Grootes et al.*, 1993].

[11] The transient glacial meltwater pulse experiment (MW) leads to a complete shutdown of the North Atlantic meridional overturning circulation (see Figure 4), a cooling of the North Atlantic by about 6–8 K (Figure 3), and a complete recovery about 200 years after the anomalous freshwater forcing has been decreased to zero. The shutdown of the THC is accompanied by an increase in Pacific warm pool salinity (see Figure 4) of about 0.3–0.5 psu. This is less than the reconstructed local millennial-scale glacial salinity changes in the Sulu Sea. Furthermore, the MW experiment simulates a bipolar seesaw response (Figure 3), similar to the reconstructed north-south temperature gradient during Heinrich events [*Stocker and Johnsen*, 2003; *Knutti et al.*, 2004].

3. Atmospheric Teleconnections

[12] In order to quantify the effect of the cold North Atlantic during the shutdown phase of the meridional overturning circulation on the global atmospheric circulation we compute the anomalies of air temperature, wind stress and evaporation minus precipitation as simulated by the MW simulation with respect to the LGM experiment as well as the anomalies simulated by the MW experiment with respect to the experiment MW2. The results (Figure 5) reveal that North Atlantic SST anomalies as depicted in Figure 3 influence the global climate. The downstream response of the North Atlantic cooling is a cooling over large parts of Asia, resulting in an enhanced meridional temperature contrast and hence a weakening of the annual mean winds over India and Southeast Asia and in particular of the summer monsoon circulation. This pronounced wind change is also reflected in an overall increase of evaporation minus precipitation in the Arabian Sea and Bay of Bengal and hence, drier conditions. This result is consistent with most recent reconstructions [*Ivanochko et al.*, 2005] of dustiness of Arabia, rainfall over India and the monsoon strength, as shown in Figure 6. In addition, we observe enhanced rainfall over evaporation in a band south of the equator in agreement with recent moisture reconstructions from northern Australia [*Turney et al.*, 2004]. Furthermore, as a result of cooling north and warming south of the equator our model simulates enhanced dryness and enhanced trade winds over northern South America. In the trade wind region also a positive air-sea feedback exists between SST, wind strength and evaporation. This model result is consistent also with the hydrological reconstructions of *Peterson et al.* [2000]. The tropical Atlantic atmospheric response to the dipole-like SST anomaly near the equator is reminiscent of a first-order baroclinic response as predicted by the *Gill* [1980] theory. Evaporation minus precipitation changes of 5–10 cm/yr can be found in the warm pool, contributing to the increase of warm pool salinity during the THC shutdown phase (Figure 4). The freshwater flux anomalies in the warm pool may originate from the relatively weak southern Indian warming (see Figure 3) during the Heinrich event. A dynamical linkage between an anomalously dry warm pool and positive Indian Ocean SST anomalies during the winter and spring season has been proposed by *Watanabe and Jin* [2003] and *Annamalei et al.* [2005]. These authors argue that an Indian Ocean warming triggers an atmospheric response in accordance with linear baroclinic first mode theory [*Gill*, 1980], which leads to a wind divergence in the warm pool area and hence to reduced precipitation. The atmospheric model employed here is capable of simulating such a kind of atmospheric response [*Timmermann et al.*, 2004] although its amplitude may be too weak, because of the quasi-geostrophic approximation and the low horizontal resolution of the model.

[13] MW2 is designed such that the atmosphere is insensitive to North Atlantic SST anomalies induced by the

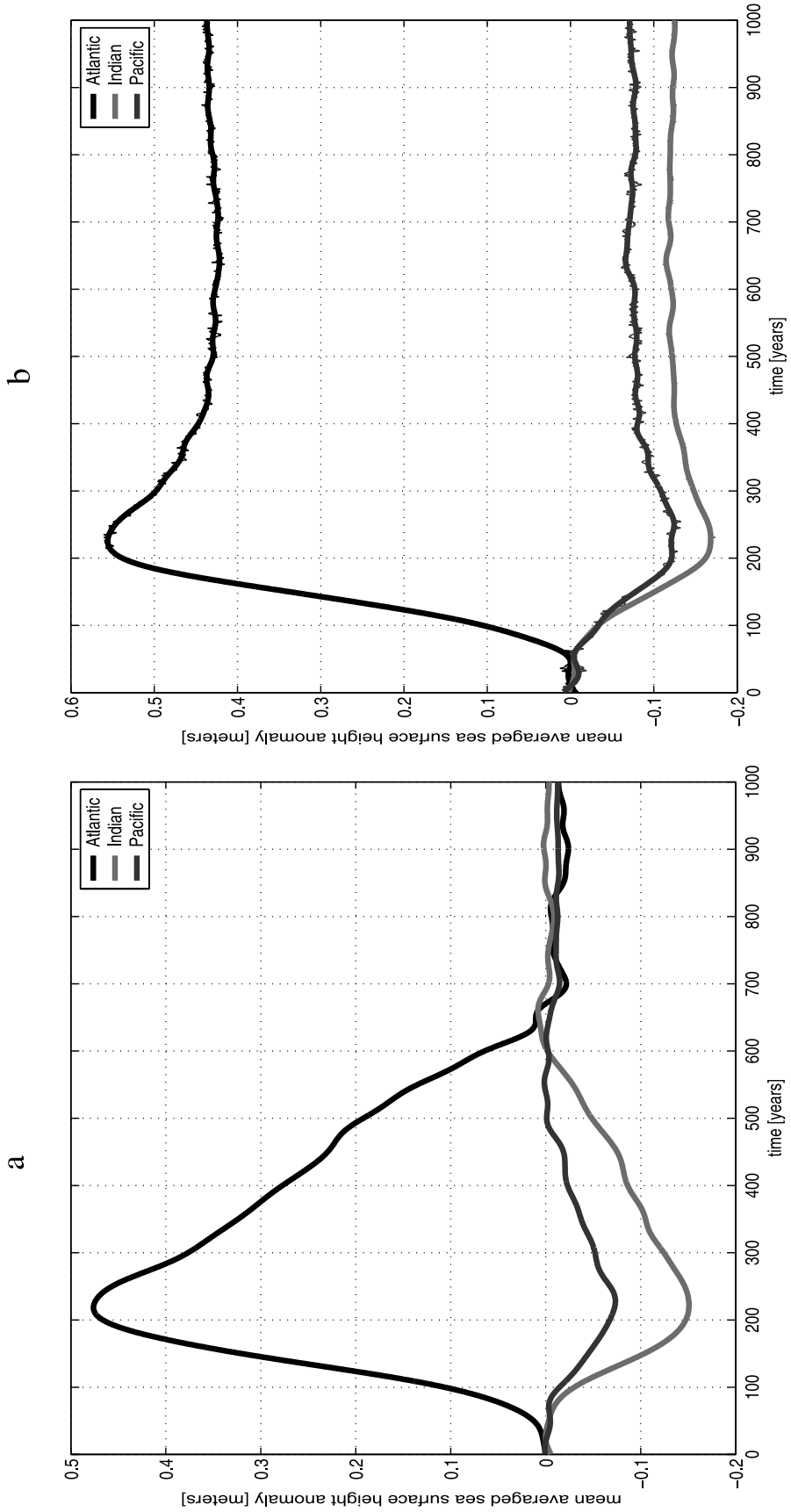

Figure 7. Global sea level seiching. (left) Basin-averaged sea level evolution (m) of the Atlantic, Pacific, and Indian ocean basins simulated by the fully coupled meltwater experiment (MW). The sea level anomalies between Atlantic and Pacific exhibit an out-of-phase relationship which is typical for standing waves, so-called global sea level seiches. (right) Same as left plot but for the global uncoupled experiment (MW1). See color version of this figure at back of this issue.

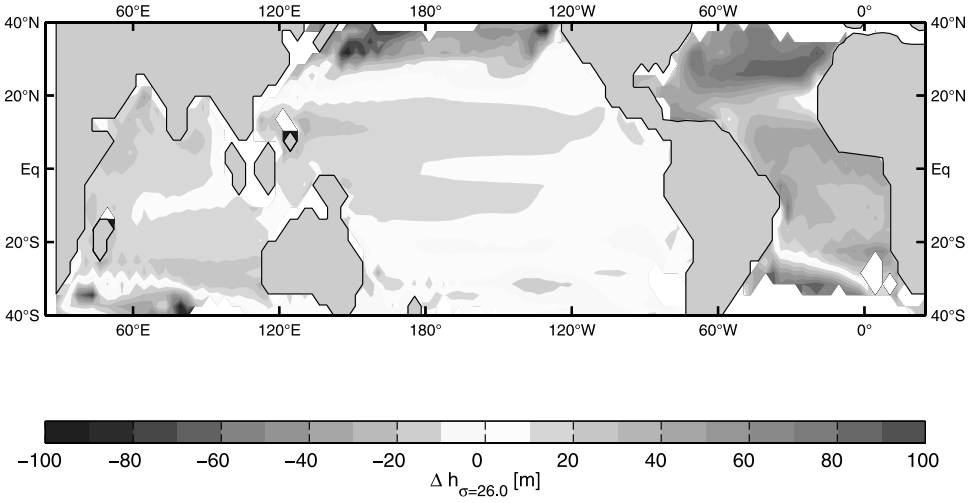

Figure 8. Thermocline response to a THC shutdown: difference of the time-averaged depth of the isopycnal 26.0 kg/m^3 surface between a collapsed THC state (years 200–300 in MW) and an uncollapsed LGM THC state (years 1–30 in MW). The 26.0 kg/m^3 isopycnal surface separates upper ocean thermocline waters from deep ocean waters. An overall deepening of the North Atlantic thermocline is accompanied by a deepening of the thermocline in the other tropical oceans. See color version of this figure at back of this issue.

shutdown of the THC. Figure 5 (left) and Figure 5 (right), showing the effect only of North Atlantic SST anomalies, are very similar, except for smaller amplitudes in the tropics, simulated by MW2. This suggests that the main anomalous features of the atmospheric circulation discussed here directly result from the North Atlantic temperature anomalies and their downstream signature, in contrast to the assumptions of *Stott et al.* [2002]. This includes not only the changes of the monsoon circulations over Asia and South America but also an overall intensification of the trade winds in the Northern Hemispheric tropical Pacific. This will result in changes of the thermocline depth in the equatorial Pacific as will be discussed further below. These results illustrate the importance of the atmospheric bridge and local air-sea interactions to spread the signal from the Atlantic into the other ocean basins, supporting the conclusions of *Dong and Sutton* [2002].

4. Oceanic Teleconnections

[14] Density changes in the North Atlantic, as simulated by the glacial meltwater experiment (MW) lead to a global readjustment of the thermohaline circulation. This readjustment is established by the propagation of coastally and equatorially trapped Kelvin waves [*Kawase*, 1987; *Hsieh and Bryan*, 1996; *Huang et al.*, 2000; *Cessi et al.*, 2004; *Johnson and Marshall*, 2002]. In coarse-resolution ocean models these waves, which establish the overall mass balance, are represented by viscous boundary waves [*Hsieh et al.*, 1983]. Their characteristics depend partially on the numerical schemes employed by the ocean model and differ somewhat from those of free Kelvin waves. However, on long timescales such as those considered here this sensitivity can be disregarded. In the present simulation these waves propagate from the North Atlantic to the equator; they are forced to travel along the equator toward the coast of Africa, where they split into a northern and southern branch. While moving poleward, they radiate Rossby waves, which readjust the interior transport of the North and South Atlantic and weaken the boundary wave amplitude. The southern wave branch travels around the southern tip of South Africa into the Indian Ocean and subsequently the Pacific Ocean. The baroclinic adjustment between Atlantic and Pacific to an initial North Atlantic density anomaly takes from a few years to decades [*Cessi et al.*, 2004].

[15] The overall sea level and thermocline depth changes can be described in terms of a standing wave pattern (Figure 7), a global seiche [*Cessi et al.*, 2004]. In agreement with *Cessi et al.* [2004], a centennial sea level rise of about 40 cm in the North Atlantic is accompanied by an almost instantaneous sea level drop of 15 and 8 cm in the Indian and Pacific ocean, respectively. The globally averaged sea level signal has been removed from our analysis. Figure 7 reveals that the THC does not recover from its forced collapse for the MW1 experiment. This is due to the lack of wind-driven transport of anomalous salinity from the tropics to the extratropics, as will be discussed in a forthcoming paper. However, during the initial shutdown stages (years 0–150), the dynamical behavior resembles that of the MW experiment. Experiment MW1 highlights not only the importance of air-sea coupling for the recovery of the THC but also the importance of oceanic wave processes in establishing large-scale panoceanic connections on centennial to millennial timescales.

[16] As predicted by simple shallow water models [*Huang et al.*, 2000] these global baroclinic readjustment processes are associated with thermocline changes in the Atlantic, the Indian and the Pacific oceans. Figure 8 shows that a collapse of the meridional overturning circulation in the North Atlantic leads to changes in the depth of iso-

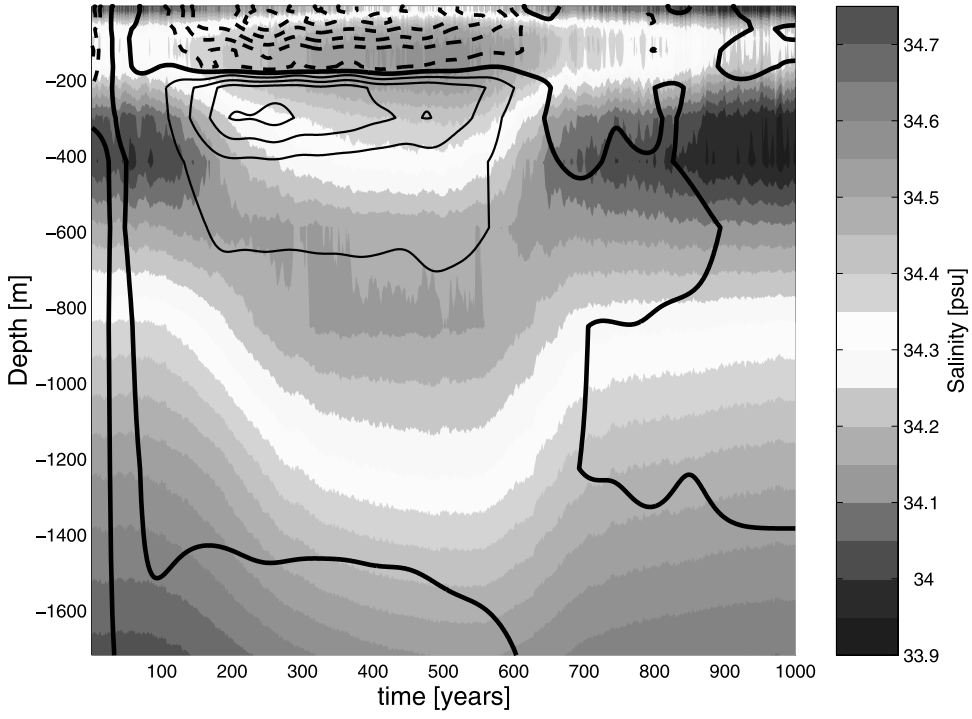

Figure 9. Mechanism for warm pool salinity changes: time-depth diagram of area-averaged salinity [psu] near the core site of MD98-2181 (shaded) and zonal currents (contour) (contour interval is 2 cm/s). See color version of this figure at back of this issue.

pycnals characterizing thermocline waters in the tropical Indian and Pacific oceans by up to 20 m, which is comparable to warm pool thermocline depth anomalies typically obtained during present-day ENSO events. However, it should be noted here that the simulated thermocline anomalies in Figure 8 originate from two sources: One is the oceanic global adjustment to North Atlantic density anomalies triggering Kelvin and Rossby waves and deepening the tropical Pacific thermocline. The other source is the equatorial trade wind intensification depicted in Figure 5 which is a direct result of hemispheric anomalies of the temperature gradient during the Heinrich event. In case the thermocline signal has an SST manifestation, local positive air-sea interactions are expected to further modify the thermocline signal. It should also be noted that the Bjerknes positive air-sea feedback in the tropical Pacific is underestimated in our coupled model. Western tropical Pacific thermocline depth anomalies in the uncoupled simulation (MW1) attain values of 5–10 m, as compared to simulated 20 m in the fully coupled MW experiment and the MW2 simulation which disregards SST anomalies in the North Atlantic.

[17] Locally, the centennial-scale density and thermocline depth anomalies in the tropical Pacific are accompanied by currents anomalies. In MW the thermocline gradients as well as the intensification of the equatorial trade winds lead to a strengthening of the South Equatorial Current as documented in Figure 9 and hence an intensification of cold and saline water advection from the eastern to the western tropical Pacific. This surface transport anomaly in the warm pool area increases the surface density of the warm pool waters, destroying the very stable stratification of the warm pool that is established by a shallow freshwater cap in both present-day and simulated glacial conditions. Salinity maxima and minima in the MW experiment (years 200–500) can be observed at depths of 150–200 m and 500–1000 m, respectively. In turn, the freshwater cap of the warm pool is mixed with cold and salty waters from below. In addition to the salinity and cold water advection due to an enhanced South Equatorial Current, the vertical mixing contributes to the generation of a positive sea surface salinity anomaly (Figure 9) of about 0.3–0.5 psu and a negative sea surface temperature anomaly of −0.6 K.

5. Summary and Discussion

[18] We studied the response of the global climate system to Heinrich events using a coupled atmosphere-ocean model of intermediate complexity. We presented modeling evidence for a rapid oceanic teleconnection between sea level variations in the glacial North Atlantic, such as those recorded e.g., during Heinrich events, and sea level variations of opposite phase in the tropical Pacific. When sea level in the North Atlantic increases because of meltwater injections, a thermocline (see Figure 8) and sea level gradient is established by baroclinic global ocean adjustment between the ocean basins that drives anomalous geostrophic surface and subsurface current anomalies and enhances the transport of cold and salty waters into the Pacific warm pool. (A part of the global oceanic standing wave travels through the Indonesian passages as an equatorial viscous boundary

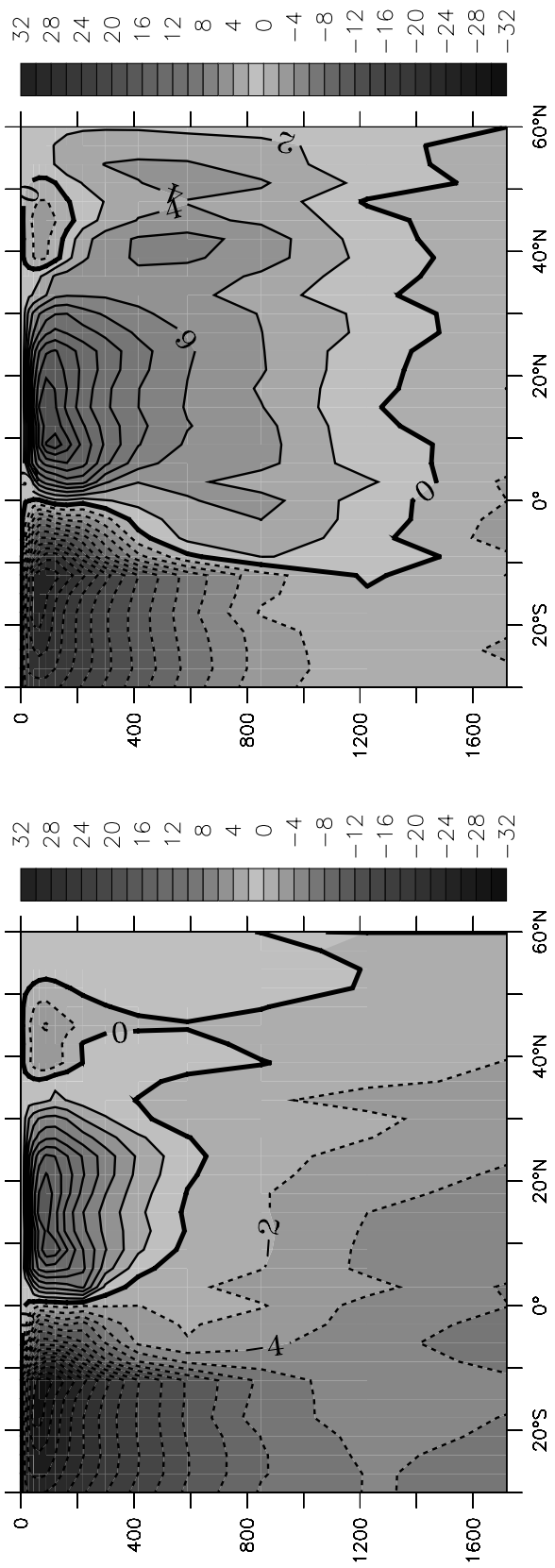

Figure 10. Panoceanic overturning seesaw. (left) Meridional stream function (Sv) of the Pacific Ocean averaged over the first 50 years of the Heinrich simulation. No significant changes of North Atlantic deepwater formation have occurred. (right) Same as left but averaged for the years 250–300 of the Heinrich simulation. Significant changes in the North Pacific occur as a result of the THC shutdown in the North Atlantic. See color version of this figure at back of this issue.

wave. Because our LGM model configuration does not take into account the drop of global sea level during glacial times and the glacial topography of the Indonesian passages is not represented precisely. The details of the wave propagation around the maritime continent may have been different during glacial periods. However, as these waves lead to an overall baroclinic sea level and density adjustment we may assume that under glacial topographic conditions also a strong large-scale connection existed between the Indian and Pacific oceans, partly provided by Kelvin waves traveling around Australia.) This effect is furthermore amplified by a trade wind intensification in the Pacific ocean and a reduction of precipitation in the Pacific warm pool, triggered by a change of the global meridional surface temperature gradient during the shutdown phase of the meridional overturning circulation. (The coupled atmosphere-ocean-sea-ice model employed here somewhat underestimates the tropical air-sea coupling [*Timmermann et al.*, 2004]. Hence the amplitude of the thermocline anomaly pattern (see Figure 8) generated during the THC shutdown phase may be too small, but its qualitative structure appears to be robust.) Furthermore, this gradient leads to a weakening of the summer monsoons over India and Southeast Asia as well as to reduced precipitation over northern South America and an intensification of precipitation over northern Australia, in accordance with recent paleoreconstructions. Further evidence supporting our conclusions comes from an analysis of reconstructed Sulu Sea surface salinity variations [*Rosenthal et al.*, 2003] during deglaciation. Sea surface salinity anomalies in this area parallel climate fluctuations in Greenland. In the MD97-2141 record from the Sulu Sea area heavy $\delta^{18}O$ values (high salinity) coincide with Heinrich event 1 and the Younger Dryas event [*Rosenthal et al.*, 2003], whereas low values are found for instance during the Bolling transition. This general panoceanic pattern of reconstructed salinity variations during the deglaciation is consistent with the proposed global teleconnection mechanism which involves both the ocean (Figure 8) and the atmosphere (Figure 5).

[19] Recently, it was found [*Saenko et al.*, 2004] that a collapse of the meridional overturning circulation in the North Atlantic may lead to the establishment of an intermediate overturning circulation in the North Pacific with deep water formation in the northern North Pacific. This North Atlantic–North Pacific seesaw effect is also simulated in our MW experiment (see Figure 10). The trigger for the generation of North Pacific Deep Water during Heinrich events is the geostrophic salinity transport induced by the quasi-stationary thermocline field that originates from the global wave adjustment in response to the North Atlantic density anomalies. The salinity increase is further amplified by the Stommel feedback [*Stommel*, 1961] as proposed by *Saenko et al.* [2004]. Hence the global thermocline adjustment induces a geostrophic salinity transport into the extratropical North Pacific. This transport destabilizes the water column by increased northward surface salinity transport (not shown) thereby generating a North Pacific intermediate overturning cell. In turn, the changed subtropical (southward shift) and supolar gyres (not shown) induce a weak warming of up to 1.5 K in the eastern North Pacific and a cooling of about −1.5 K in the northwestern Pacific Kuroshio extension region (see Figure 3). The reconstructed North Pacific warming of about 3–6 K [*Kiefer et al.*, 2001] is not simulated as a large-scale feature here. In a forthcoming study we will address the question whether a possible future weakening of the thermohaline circulation due to greenhouse warming may have a similar influence on global thermocline patterns [*Hsieh and Bryan*, 1996], tropical climate and ENSO variability.

[20] Our modeling results suggest the global pattern of millennial-scale climate change can be explained without invoking a link between El Niño and stadials [*Stott et al.*, 2002], although our study does not exclude this possibility. Previous findings from paleoreconstructions can be explained in terms of North Atlantic forcing only. Our coupled global climate model simulations suggest that salinity variations in the warm pool vary in concert with North Atlantic temperature anomalies. Warm pool salinity anomalies originate from salinity advection triggered by wind and thermocline anomalies as well as from freshwater flux changes originating from SST anomalies in the Indian Ocean and a large-scale reorganization of the ITCZ.

[21] **Acknowledgments.** U. Krebs, F. Justino, and A. Timmermann were supported from the Collaborative Research Project SFB460 of the Deutsche Forschungsgemeinschaft. A. Timmermann has been further supported by the Japan Agency for Marine-Earth Science and Technology (JAMSTEC) through its sponsorship of the International Pacific Research Center. We are grateful to Lowell Stott for his very valuable and constructive comments on an earlier version of the manuscript. We also thank Gisela Speidel for her careful editing of an earlier version of the manuscript.

References

Annamalei, H., P. Liu, and S.-P. Xie (2005), Southwest Indian Ocean SST variability: Its local effect and remote influence on Asian monsoons, *J. Clim.*, in press.

Bard, E. (2001), Comparison of alkenones estimates with other paleotemperature proxies, *Geochem. Geophys, Geosyst.*, *2*, 1–12.

Blunier, T., and E. Brook (2001), Timing of millennial-scale climate change in Antarctica and Greenland during the last glacial period, *Science*, *291*, 109–112.

Campin, J. M., and H. Goosse (1999), A parameterization of dense overflow in large-scale ocean models in *z* coordinate, *Tellus, Ser. A*, *51*, 412–430.

Cane, M., and A. C. Clement (1999), A role for the tropical Pacific coupled ocean-atmosphere system on Milankovitch and millennial timescales. part II, Global impacts, in *Mechanisms of Global Climate Change at Millennial Time Scales*, *Geophys. Monogr. Ser.*, vol. 112, edited by P. U. Clark, R. S. Webb, and L. D. Keigwin, pp. 59–61, AGU, Washington, D. C.

Cessi, P., K. Bryan, and R. Zhang (2004), Global seiching of thermocline waters between the Atlantic and the Indian-Pacific Ocean basins, *Geophys. Res. Lett.*, *31*, L04302, doi:10.1029/2003GL019091.

Climate: Long-Range Investigation, Mapping, and Prediction (CLIMAP) (1981), Seasonal reconstruction of the Earth's surface of the Last Glacial Maximum, *Geol. Soc. Am. Map. Chart Ser., MC-36*.

Crowley, T. J., and S. K. Baum (1997), Effect of vegetation on an ice-age climate model simulation, *J. Geophys. Res.*, *102*, 16,463–16,480.

Dansgaard, W., et al. (1993), Evidence for general instability of past climate from a 250-kyr ice-core record, *Nature*, *364*, 218–220.

Dong, B. W., and R. T. Sutton (2002), Adjustment of the coupled ocean–atmosphere system to a sudden change in the thermohaline circulation, *Geophys. Res. Lett.*, *29*(15), 1728, doi:10.1029/2002GL015229.

Gent, P. R., and J. C. McWilliams (1990), Isopycnal mixing in ocean general circulation model, *J. Phys. Oceanogr.*, *20*, 150–155.

Gill, A. E. (1980), Some simple solutions for heat-induced tropical circulation, *Q. J. R. Meteorol. Soc.*, *106*, 447–462.

Goosse, H., and T. Fichefet (1999), Importance of ice-ocean interactions for the global ocean circulation: A model study, *J. Geophys. Res.*, *104*, 23,337–23,355.

Goosse, H., E. Deleersnijder, T. Fichefet, and M. H. England (1999), Sensitivity of a global coupled ocean-sea ice model to the parameterization of vertical mixing, *J. Geophys. Res.*, *104*, 13,681–13,695.

Grootes, P. M., M. Stuiver, J. W. C. White, S. J. Johnsen, and J. Jouzel (1993), Comparison of oxygen isotope records from the GISP2 and GRIP Greenland ice cores, *Nature*, *366*, 552–554.

Heinrich, H. (1988), Origin and consequences of cyclic ice rafting in the northeast Atlantic Ocean during the past 130,000 years, *Quat. Res.*, *29*, 143–152.

Held, I. M., and M. J. Suarez (1978), A two-level primitive equation atmospheric model designed for climate sensitivity experiments, *J. Atmos. Sci.*, *35*, 206–229.

Honjo, S., J. Dymond, W. Prell, and V. Ittekot (1999), Monsoon-controlled export fluxes to the interior of the Arabian Sea, *Deep Sea Res., Part II*, *46*, 1859–1902.

Hostetler, S. W., and A. C. Mix (1999), Reassessment of ice-age cooling of the tropical ocean and atmosphere, *Nature*, *399*, 673–676.

Hsieh, W. W., and K. Bryan (1996), Redistribution of sea level rise associated with enhanced greenhouse warming: A simple model study, *Clim. Dyn.*, *12*, 535–544.

Hsieh, W. M., M. K. Davey, and R. C. Wajsowicz (1983), The free Kelvin wave in finite-difference numerical models, *J. Phys. Oceanogr.*, *13*, 1381–1397.

Huang, R. X., M. A. Cane, N. Naik, and P. Goodman (2000), Global adjustment of the thermocline in response to deepwater formation, *Geophys. Res. Lett.*, *27*, 759–762.

Ivanochko, T. S., R. S. Ganeshram, G. J. A. Brummer, G. Ganssen, S. J. A. Jung, S. G. Moreton, and D. Kroon (2005), Variations in tropical convection as an amplifier of global climate change at the millennial scale, *Earth. Planet. Sci. Lett.*, *253*, 302–314.

Johnson, H., and D. P. Marshall (2002), A theory for the surface Atlantic response to thermohaline variability, *J. Phys. Oceanogr.*, *32*, 1121–1132.

Kawase, M. (1987), Establishment of deep ocean circulation driven by deep-water production, *J. Phys. Oceanogr.*, *17*, 2294–2317.

Keigwin, L. D., and S. J. Lehman (1994), Deep circulation change linked to Heinrich event 1 and Younger Dryas in a middepth North Atlantic core, *Paleoceanography*, *9*, 185–194.

Kiefer, T., M. Sarnthein, H. Erlenkeuser, P. M. Grootes, and A. P. Roberts (2001), North Pacific response to millennial-scale changes in ocean circulation over the last 60 kyr, *Paleoceanography*, *16*, 179–189.

Kitoh, A., S. Muakami, and H. Koide (2001), A simulation of the Last Glacial Maximum with a coupled atmosphere-ocean GCM, *Geophys. Res. Lett.*, *28*, 2221–2224.

Knutti, R., J. Flückiger, T. Stocker, and A. Timmermann (2004), Strong hemispheric coupling of glacial climate through freshwater discharge and ocean circulation, *Nature*, *430*, 851–856.

Koutavas, A., J. Lynch-Stieglitz Jr., T. M. Marchitto, and J. P. Sachs (2002), El Niño-like pattern in ice age tropical Pacific sea surface temperature, *Science*, *297*, 226–230.

Lang, C., M. Leuenberger, J. Schwander, and S. Johnsen (1999), 16°C rapid temperature variation in central Greenland 70,000 years ago, *Science*, *286*, 934–937.

Lea, D. W., D. K. Pak, and H. J. Spero (2000), Climate impact of late Quaternary equatorial Pacific sea surface temperature variations, *Science*, *289*, 1719–1724.

Livezey, R. E., M. Masutani, A. Leetmaa, H. Rui, M. Ji, and A. Kumar (1997), Teleconnective response of the Pacific–North American region atmosphere to large central equatorial Pacific SST anomalies, *J. Clim.*, *10*, 1787–1820.

Lyle, M., F. Prahl, and M. Sparrow (1992), Upwelling and productivity changes inferred from a temperature record in the equatorial Pacific, *Nature*, *355*, 812–815.

Marshall, J., and F. Molteni (1993), Toward a dynamic understanding of planetary-scale flow regimes, *J. Atmos. Sci.*, *50*, 1792–1818.

Mellor, G. L., and T. Yamada (1982), Development of a turbulence closure model for geophysical fluid problems, *Rev. Geophys.*, *20*, 851–875.

Opsteegh, J. D., R. J. Haarsma, F. M. Selten, and A. Kattenberg (1998), ECBILT, A dynamic alternative to mixed boundary conditions in ocean models, *Tellus, Ser. A*, *50*, 348–367.

Peltier, W. R. (1994), Ice age paleotopography, *Science*, *265*, 195–201.

Peterson, L. C., G. H. Haug, K. A. Hughen, and U. Rohl (2000), Rapid changes in the hydrologic cycle of the tropical Atlantic during the last glacial, *Science*, *290*, 1947–1951.

Rahmstorf, S. (2003), Timimg of abrupt climate change: A precise clock, *Geophys. Res. Lett.*, *30*(10), 1510, doi:10.1029/2003GL017115.

Roche, D., D. Paillard, and E. Cortijo (2004), Constraints on the duration and freshwater release of Heinrich event 4 through isotope modeling, *Nature*, *432*, 379–382, doi:10.1038/nature03059.

Rosenthal, Y., D. W. Oppo, and B. K. Linsley (2003), The amplitude and phasing of climate change during the last deglaciation in the Sulu Sea, western equatorial Pacific, *Geophys. Res. Lett.*, *30*(8), 1428, doi:10.1029/2002GL016612.

Saenko, O. A., A. Schmittner, and A. J. Weaver (2004), The Atlantic-Pacific seesaw, *J. Clim.*, *17*, 2033–2038.

Sarnthein, M., U. Pflaumann, and M. Weinelt (2003), Past extent of sea ice in the northern North Atlantic inferred from foraminiferal paleotemperature estimates, *Paleoceanography*, *18*(2), 1047, doi:10.1029/2002PA000771.

Schultz, H., H. Erlenkeuser, and U. von Rad (1998), Correlation between Arabian Sea and Greenland climate oscillations of the past 110,000 years, *Nature*, *393*, 54–57.

Severinghaus, J. P., and E. J. Brook (1999), Abrupt climate change at the end of the last glacial period inferred from trapped air in polar ice, *Science*, *286*, 930–934.

Shackleton, N. J., M. A. Hall, and E. Vincent (2000), Phase relationships between millennial-scale events 64,000 to 24,000 years ago, *Paleoceanography*, *15*, 565–569.

Sidall, M., E. J. Rohling, A. Almogi-Labin, C. Hemleben, D. Meischners, I. Schmelzer, and D. A. Smeed (2003), Sea-level fluctuations during the last glacial cycle, *Nature*, *423*, 853–858.

Stocker, T. F., and S. J. Johnsen (2003), A minimum thermodynamic model for the bipolar seesaw, *Paleoceanography*, *18*(4), 1087, doi:10.1029/2003PA000920.

Stommel, H. M. (1961), Thermohaline convection with two stable regimes of flow, *Tellus*, *13*, 224–230.

Stott, L., C. Poulsen, S. Lund, and R. Thuell (2002), Super ENSO and global climate oscillations at millennial time scales, *Science*, *297*, 222–226.

Timmermann, A., M. Schulz, H. Gildor, and E. Tziperman (2003), Coherent resonant millennial-scale climate oscillations triggered by massive meltwater pulses, *J. Clim.*, *16*, 2569–2585.

Timmermann, A., F. Justino, F.-F. Jin, U. Krebs, and H. Goosse (2004), Surface temperature control in the north and tropical Pacific during the last glacial maximum, *Clim. Dyn.*, *23*, 353–370.

Turney, C. S., A. P. Kershaw, S. C. Clemens, N. Branch, P. T. Moss, and K. Fifield (2004), Synchronous millennial-scale climatic oscillations of the tropical Pacific and north Atlantic Oceans, *Nature*, *428*, 306–309.

Watanabe, M., and F.-F. Jin (2003), A moist linear baroclinic model: Coupled dynamical-convective response to El Niño, *J. Clim.*, *16*, 1121–1139.

Yokoyama, Y., T. M. Esat, and K. Lambeck (2001), Coupled climate and sea-level changes deduced from Huan Peninsula coral terraces of the last ice age, *Earth Planet. Sci. Lett.*, *193*, 579–587.

H. Goosse, Institut d'Astronomie et de Géophysique, Université Catholique de Louvain, 1348 Louvain-la-Neuve, Belgium.

T. Ivanochko, Department of Earth and Ocean Sciences, University of British Columbia, Vancouver, British Columbia, Canada V6T 1Z4.

F. Justino, Department of Physics, University of Toronto, Toronto, Ontario, Canada M5S 1A7.

U. Krebs, Leibniz Institut für Meereswissenschaften, IfM-GEOMAR, D-24148 Kiel, Germany.

A. Timmermann, International Pacific Research Center, SOEST, University of Hawai'i, 1680 East-West Road, Honolulu, HI 96822, USA. (axel@hawaii.edu)

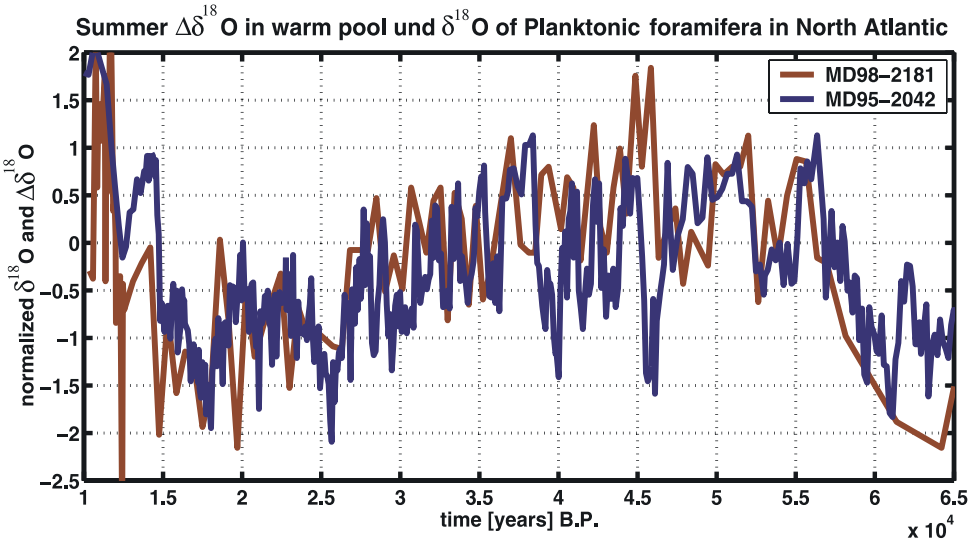

Figure 1. Extratropical-tropical connections: normalized and inverted time series of $\Delta\delta^{18}O$ of planktonic foramanifera (red) in the Pacific warm pool core MD98-2181 [*Stott et al.*, 2002]. The largest $\Delta\delta^{18}O$ variations for Globigerinoides ruber represent local salinity variations and are coherent with the Dansgaard-Oeschger (DO) cycles, as recorded in the normalized $\delta^{18}O$ of planktonic foraminifera (blue) sampled off the Iberian margin [*Shackleton et al.*, 2000]. Both records are shown on the Greenland Ice Sheet Project 2 (GISP2) timescale [*Blunier and Brook*, 2001].

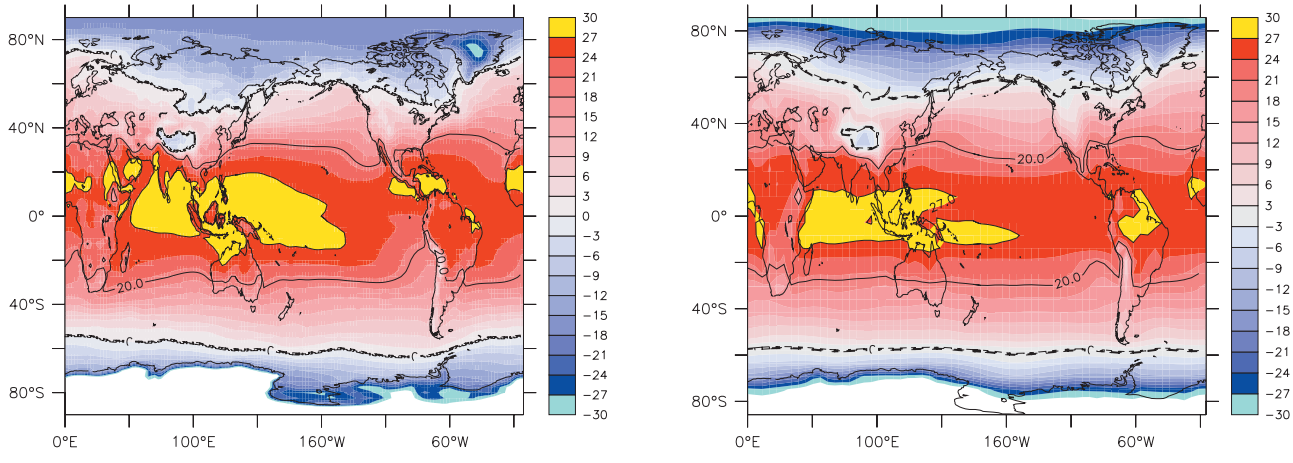

Figure 2. (left) Averaged ECMWF Reanalysis Data-Assimilation 40 (ERA40) 2-m temperature, representing an estimate of the observed temperatures. (right) Simulated averaged 2-m temperature for a 280 ppm 2000-year-long control (CTR) simulation using ECBilt-Clio.

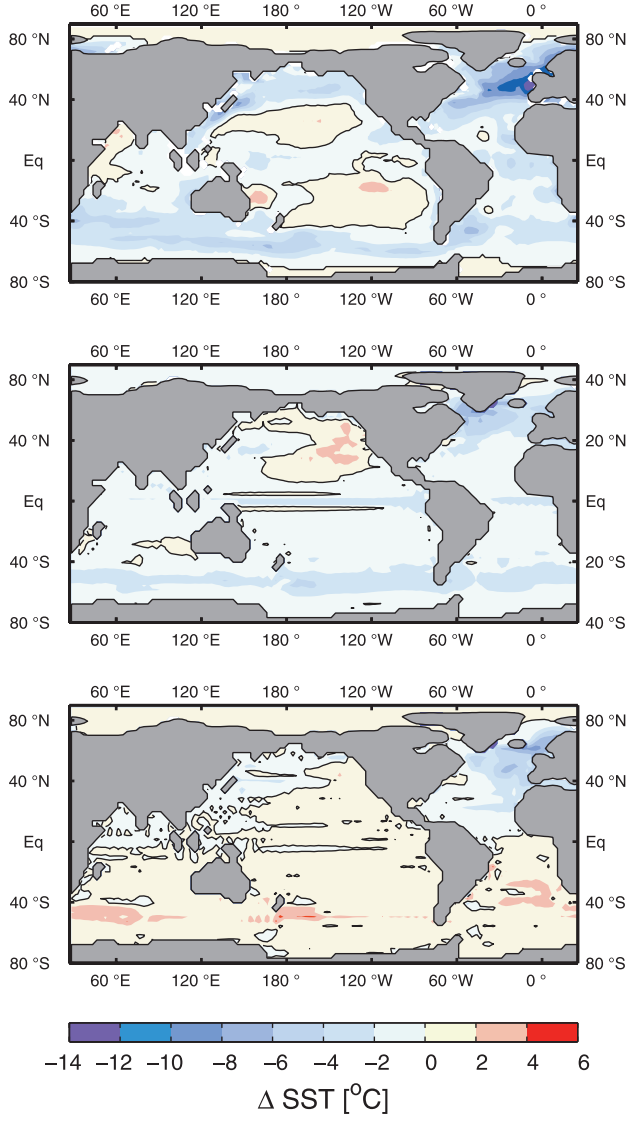

Figure 3. Reconstructed and simulated glacial sea surface temperature (SST) anomalies. (top) Difference between reconstructed North Atlantic GLAMAP [*Sarnthein et al.*, 2003] and Pacific and Indian oceans [*CLIMAP*, 1981] sea surface temperature (time average of February and August) for the Last Glacial Maximum (LGM) and the present-day SST [*CLIMAP*, 1981]. (middle) Sensitivity of the simulated annual mean SST to glacial boundary conditions as quantified by the difference of the equilibrated time-mean SST of the LGM experiment and the preindustrial CTR experiment. (bottom) Simulated SST difference between a collapsed thermohaline circulation (THC) state during the LGM (time average of years 200–300 in experiment meltwater (MW)) and normal LGM conditions.

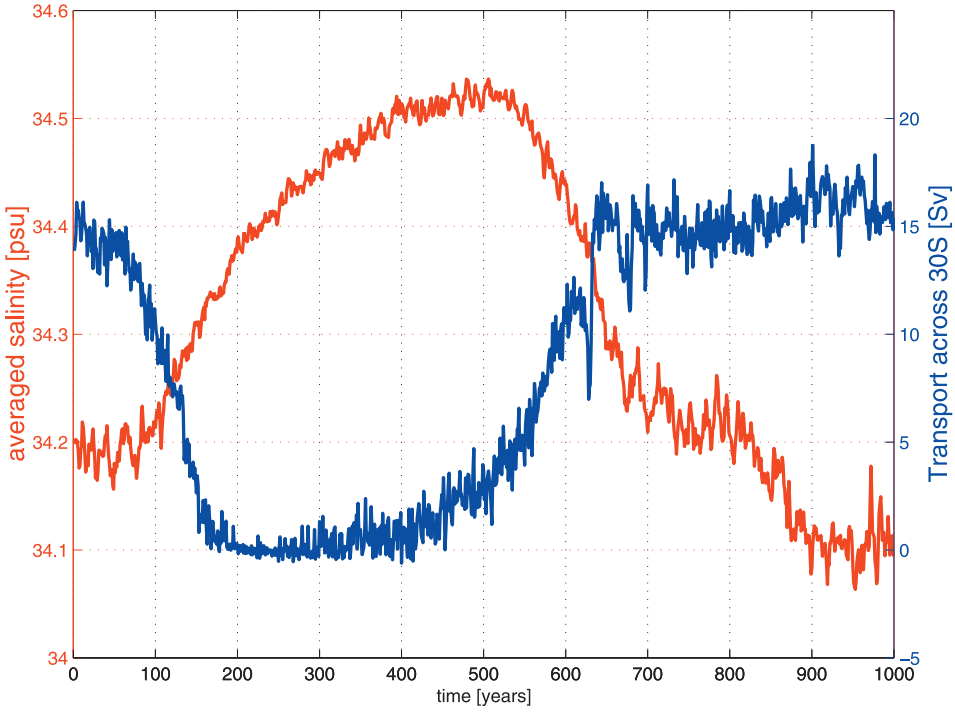

Figure 4. North Atlantic–tropical Pacific teleconnections. Simulated time series of the meridional ocean transport across 30°S in the North Atlantic (Sv = $10^6 \times m^3/s$) (blue) and area-averaged salinity (psu) in the Pacific warm pool (15°S–15°N, 120°E–160°E) area are shown.

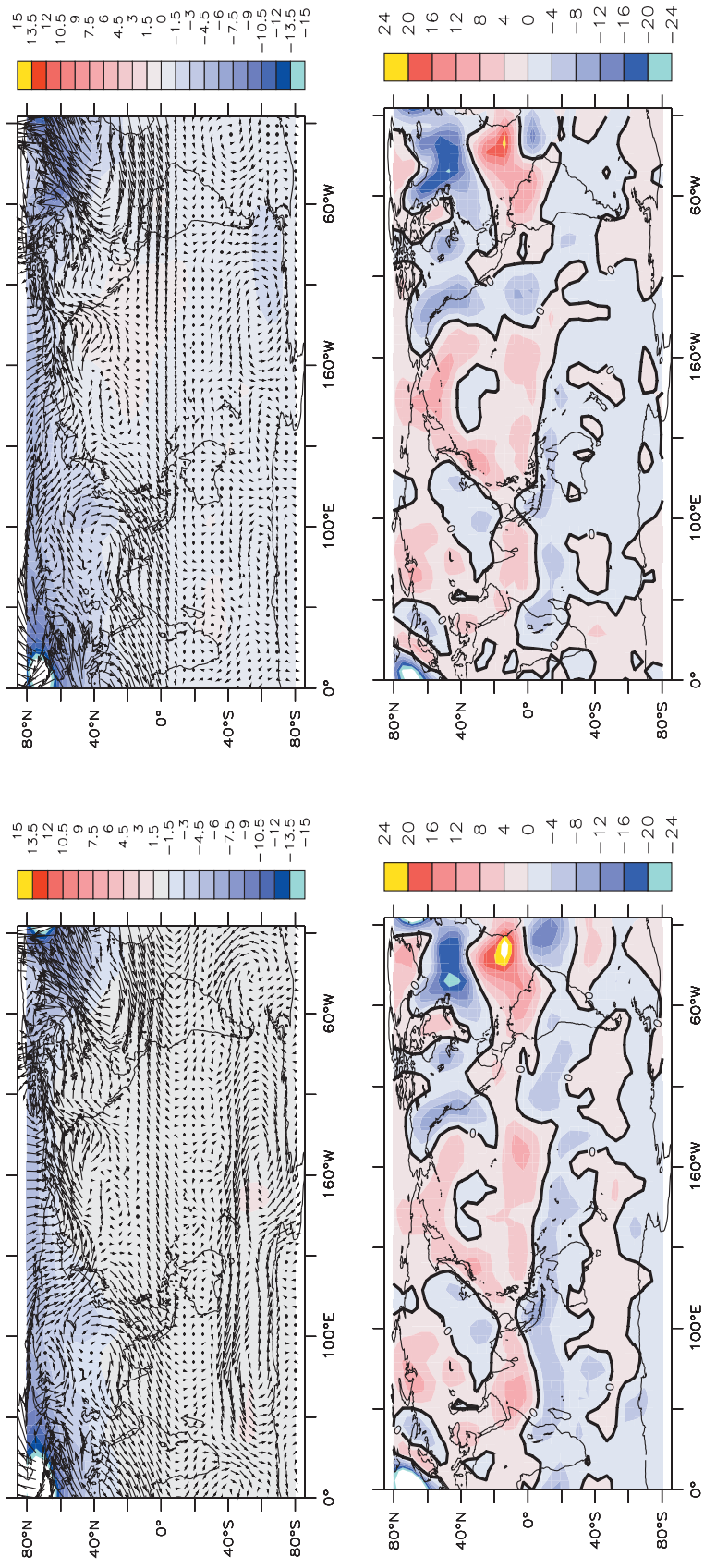

Figure 5. Atmospheric response to Heinrich event. (top) Difference of time-averaged wind stress (vectors) and temperature (shading) fields of (left) MW and LGM and (right) MW and MW2. The time average represents the THC shutdown state and is computed from the simulation years 250–300. (bottom) Same as top plots but for evaporation minus precipitation (cm/yr).

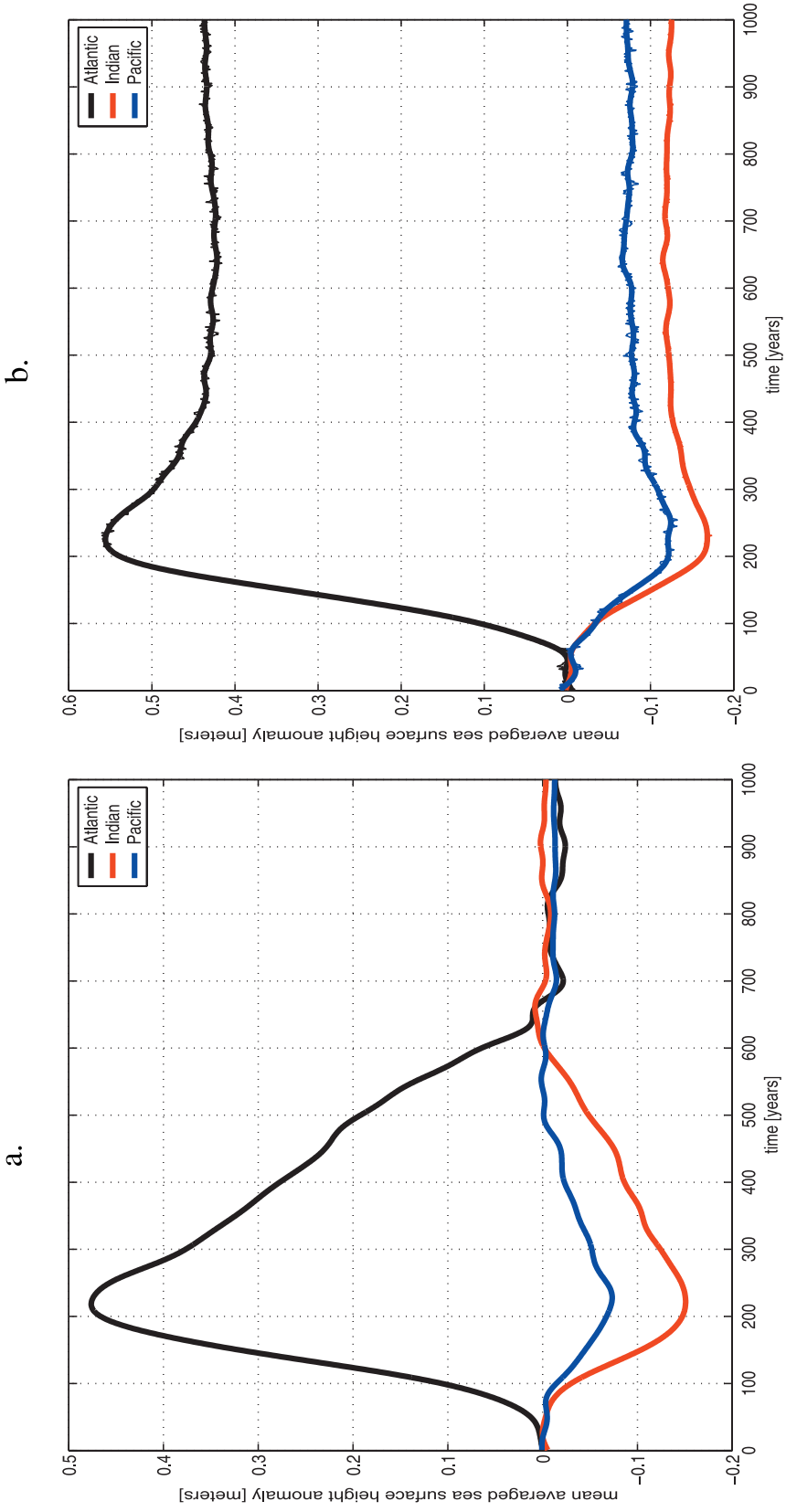

Figure 7. Global sea level seiching. (left) Basin-averaged sea level evolution (m) of the Atlantic, Pacific, and Indian ocean basins simulated by the fully coupled meltwater experiment (MW). The sea level anomalies between Atlantic and Pacific exhibit an out-of-phase relationship which is typical for standing waves, so-called global sea level seiches. (right) Same as left plot but for the global uncoupled experiment (MW1).

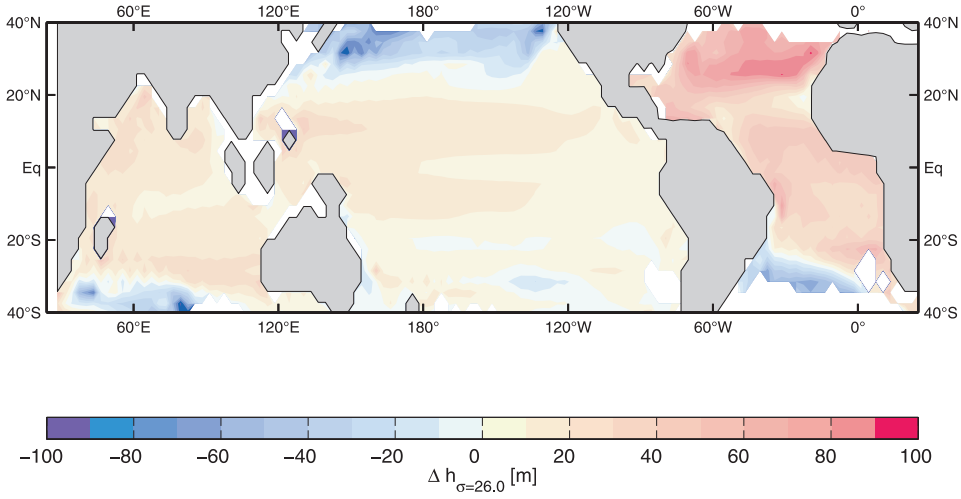

Figure 8. Thermocline response to a THC shutdown: difference of the time-averaged depth of the isopycnal 26.0 kg/m^3 surface between a collapsed THC state (years 200–300 in MW) and an uncollapsed LGM THC state (years 1–30 in MW). The 26.0 kg/m^3 isopycnal surface separates upper ocean thermocline waters from deep ocean waters. An overall deepening of the North Atlantic thermocline is accompanied by a deepening of the thermocline in the other tropical oceans.

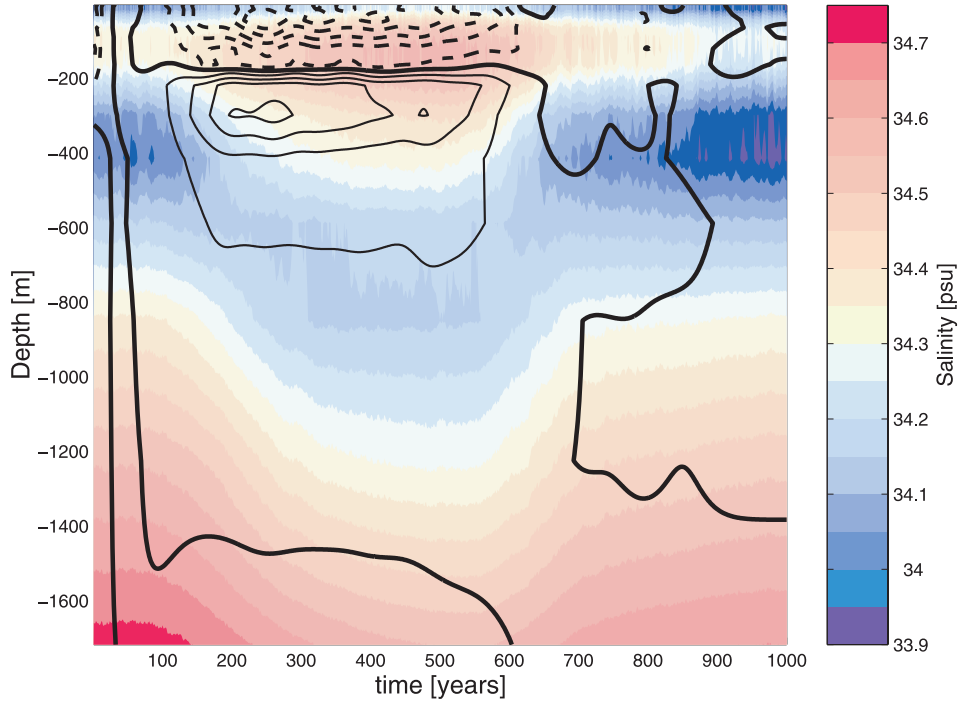

Figure 9. Mechanism for warm pool salinity changes: time-depth diagram of area-averaged salinity [psu] near the core site of MD98-2181 (shaded) and zonal currents (contour) (contour interval is 2 cm/s).

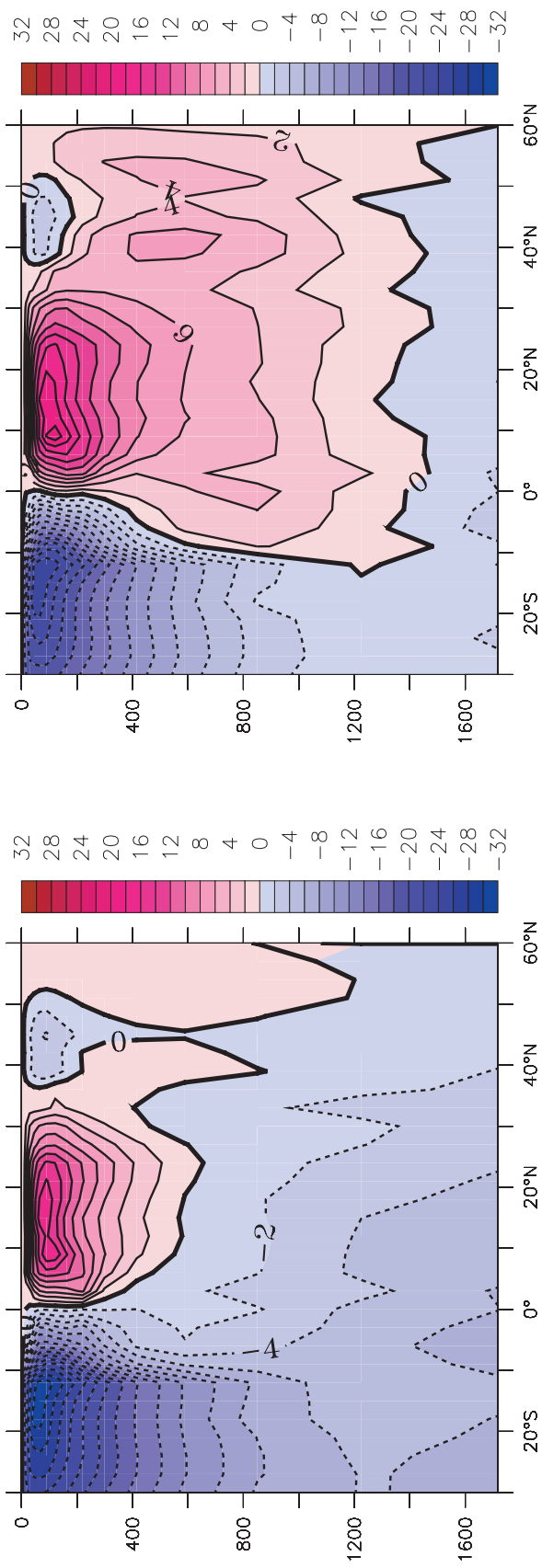

Figure 10. Panoceanic overturning seesaw. (left) Meridional stream function (Sv) of the Pacific Ocean averaged over the first 50 years of the Heinrich simulation. No significant changes of North Atlantic deepwater formation have occurred. (right) Same as left but averaged for the years 250–300 of the Heinrich simulation. Significant changes in the North Pacific occur as a result of the THC shutdown in the North Atlantic.